Journal of Materials Chemistry B

Accepted Manuscript

ROYAL SOCIETY OF CHEMISTRY

www.rsc.org/materialsB

Journal of Materials Chemistry B

RSCPublishing

ARTICLE

Effects of Plasma-Generated Nitrogen Functionalities on Upregulation of Osteogenesis of Bone Marrow-Derived Mesenchymal Stem Cells†

Wei Zhang,[a,*] Jun Liu,[a] Haigang Shi,[a] Na Liu,[b] Kun Yang,[a] Lianxin Shi,[a] Bin Gu,[b] Huaiyu Wang,[c] Junhui Ji,[a,*] Paul K. Chu[c]

Cite this: DOI: 10.1039/x0xx00000x

Received 00th January 2012,
Accepted 00th January 2012

DOI: 10.1039/x0xx00000x

www.rsc.org/MaterialsB

Because of the complex plasma reactions and chemical structure of polymers, it is difficult to construct nitrogen functionalities controllably by plasma technology to attain the desirable biological outcome and hence, the effects of them on bone cells are sometimes ambiguous and even contradictory. In this study, argon plasma treatment is utilized to convert complex molecular chains into a pyrolytic carbon structure which possesses excellent cytocompatibility. The pyrolytic carbon then serves as a platform to prepare the designed nitrogen functionalities by nitrogen and hydrogen plasma immersion ion implantation. Primary, secondary, and tertiary amine groups can be produced selectively thus minimizing the chemical complexity and creation of multiple types of nitrogen functional groups that are often obtained by other fabrication methods. As a result of the excellent control of the nitrogen functionalities rendered by this plasma technique, the effects of individual nitrogen functionalities on the cytocompatibility and upregulation of bone marrow-derived mesenchymal stem cells (BMSCs) osteogenesis can be investigated systematically. The tertiary amine functionalities exhibit the optimal efficiency pertaining to the modulation of biological response, enhancement of osteogenesis related genes/protein expression, and calcification of the contacted BMSCs. Our results demonstrate that simple plasma technology can be conveniently employed to create the desirable nitrogen functionalities on orthopedic polymers to facilitate osseointegration and mitigate foreign body reactions.

Introduction

Orthopedic polymers such as ultra-high molecular weight polyethylene, polyamide, and polyetheretherketone are popular in bone graft substitutes[1, 2] but their poor osteoinductivity may compromise osseointegration with bone tissues.[3, 4] Since the revelation that extrinsic signals provided to bone marrow-derived mesenchymal stem cells (BMSCs) from the surface biochemical microenvironment are essential in guiding the phenotype,[5, 6] the focus is to promote the osteoinductivity of orthopedic polymers by modifying the surface chemical groups.[6-8] Generally, small osteoinductive molecules are grafted onto the bulk[9] and surface[5, 10] or coated physically[11, 12] and chemically.[5] As biomechanics and biological safety must also be considered, surface modification, especially plasma surface modification, is a viable approach.[13-16] Various plasma techniques have been utilized to modify the surface chemistry to direct BMSCs proliferation and differentiation as well as extracellular matrix production and organization.[12, 16-18] For instance, a nitrogen plasma modified surface can serve as a powerful microenvironment to modulate osteogenic differentiation of osteoblasts.[13, 19-21] However, the inherently complicated chemical structure of many biopolymers containing C-H, C-O, C=O, C-N, and N-H bonds makes it difficult to precisely construct the specific nitrogen functionalities to attain the optimal biological outcome. As a result, previous results concerning the effects of nitrogen functionalities such as primary, secondary, and tertiary amines on bone cells are ambiguous and sometimes contradictory.[19, 21-24] In this paper, a strategy to controllably construct nitrogen functionalities on polymers by plasma immersion ion implantation is described with the objective to promote the osteogenesis capacity of orthopedic polymers. Argon plasma treatment is employed to convert the molecular chains to pyrolytic carbon with excellent cytocompatibility.[25] The pyrolytic carbon subsequently serves as the platform to prepare the designed nitrogen functionalities including primary, secondary, and tertiary amines by a series of nitrogen and hydrogen plasma immersion ion implantation (PIII) steps. The effects of these nitrogen functionalities on osteogenic differentiation of BMSCs and underlying mechanism are studied and discussed.

Materials and methods

Preparation of nitrogen functionality

Polyethylene (PE, Lucoil Chemical, Grade 277-73) samples with dimensions of 10 cm × 10 cm × 0.5 mm were ion implanted using a Kauffman ion source. Argon was introduced into the ion source and argon ions were plasma implanted at a fluence of 6.14×10^{15} ions/cm^2 into the PE at 5 kV for 10 min. Argon was replaced with nitrogen and nitrogen PIII was conducted at the same ion implant fluence. Afterwards, hydrogen PIII (1.5×10^{15} ions/cm^2 or 12.28×10^{15} ions/cm^2) was performed again. The samples remained in vacuum for 10 min. The base vacuum and working pressure were less than 1.0×10^{-5} Pa and 2.0×10^{-2} Pa, and all the gases have high purity (99.99%). The only argon PIII PE was denoted as PAr, and the argon and nitrogen PIII PE was denoted as PArN, whereas PE undergoing additional hydrogen PIII with fluencies of 1.5×10^{15} ions/cm^2 and 12.28×10^{15} ions/cm^2 were designated as PArNH and PArNH$_2$, respectively.

Surface physicochemical characterization

The Raman spectra and attenuated total-reflection Fourier transform infrared spectra (ATR-FTIR) were acquired on the inVia-Reflex (Renishaw) at an excitation wavelength of 532 nm and Excalibur 3100 (Varian), respectively. The elemental chemical composition and chemical structure were determined by X-ray photoelectron spectroscopy (XPS, PHI QUANTERA II equipped with a monochromatic Al K_α source) at a pass energy (Ep) of 280 eV for wide scans and 26 eV for fine scans, resulting in instrumental resolution of 1.00 eV for wide scans and 0.025 eV for fine scans. The data were collected at a take-off angle of 45° and data analysis and multi-peak fitting were performed by the Multipak software. Time-of-flight secondary ion mass spectrometry (TOF-SIMS) was conducted on the TOF-SIMS V (ION-TOF GmbH) with 30 keV Bi_n^+ as the primary ion source. The positive spectra were obtained from 500 × 500 μm^2 areas by focusing the Bi^+ primary ions (less than 0.01 pA of pulsed current) in the "burst alignment" mode at the 10 kHz pulsing rate and 120-130 ns pulse width. The surface morphology was determined by atomic force microscopy (AFM, Multimode 8, Bruker) employing the tapping mode on a RTESPA (Bruker) probe in air at room temperature.

Bone marrow-derived mesenchymal stem cells culture

The BMSCs were provided by the Academy of Military Medical Sciences (Beijing, China). The cells were seeded in a 75 cm^2 culture flask (Corning, Lowell, MA, USA) and cultured in a humidified atmosphere (95% air, 5% CO_2) at 37 °C in Dulbecco's modified Eagle's medium (DMEM) containing 10% fetal bovine serum (FBS) (GIBCO), 100 U/mL penicillin, and 100 μg/mL streptomycin (GIBCO). The cells were refreshed every 2 days and maintained in the primary culture for 5 to 6 days. When the cells reached confluence, they were trypsinized and placed on new culture plates.

Cell cycle and apoptosis analysis

The BMSCs were cultured on tissue culture plastic (noted as Blank), PE, PArN, PArNH, and PArNH$_2$. Five groups of BMSCs were harvested at day 1 and day 3 and the cells were treated with or without 5 μM 7-xylosyl-10-deacetylpaclitaxel. After incubation for 24 h, the cells were collected and stained with 50 μg/ml DAPI (Partec, Munster, Germany). The cell cycle distribution of 1×10^5 cells was determined by flow cytometry (FCM, Partec) and cell cycle analysis was conducted using FloMax software. The fractions of cells in the G0/G1, G2/M, and S phases of the cell cycle and proliferation index (PI) were analyzed. Apoptosis was monitored using the Annexin V-FITC/PI kit (Partec) according to the manufacturer's instructions. Ten thousand cells were acquired and analyzed by FCM and FloMax software (Partec).

Quantitative real time-polymerase chain reaction

The total RNA was isolated from BMSCs using the Trizol reagent (Invitrogen). Approximately 2-5 μg of the total RNA were converted to cDNA using the Super Script First Strand Synthesis kit (Invitrogen). The quantitative real time-polymerase chain reactions were performed using the QuantiTect SYBR Green PCR kit (Toyobo, Osaka, Japan) and Applied Biosystems 7500 Real-time PCR Detection System. Three independent experiments were performed for each reaction. The primers of these gene were as follows:
RUNX 2: (F) 5′ AGGGCGCATTCCTCATCCCAGT 3′, (R) 5′-AAGACAGCGGCGTGGTGGAA 3′; OCN: (F) 5′-TGGCACCACCGTTTAGGGCA 3′, (R) 5′ TTTGGAGCAGCTGTGCCGTC 3′; BMP 2: (F) 5′ CACGAGAATGGACGTGCCC 3′, (R) 5′-GCAACACTAGAAGACAGCGG-3′. GAPDH: (F) 5′-GGCACAGTCAAGGCTGAGAATG-3′, (R) 5′-ATGGTGGTGAAGACGCCAGTA-3.

Western blot analysis of osteogenic proteins

The whole cell lysates were extracted by the lysis buffer (Raybiotech) for western blotting and the protein content of the lysate was determined using a protein assay kit (Beyotime) according to the manufacturer's recommended protocol. The proteins were loaded on 10% SDS polyacrylamide gels, transferred to PVDF membranes (Millipore, Billerica, MA), and blocked with 5% nonfat milk powder in PBST (phosphate-buffered saline with 0.1% Tween). The membranes were probed overnight with the following monoclonal primary antibodies: anti-Runx2 (Abcam, Cambridge, UK, 3 μg/ml) and OCN (Abcam, 1:800), and monoclonal antibodies against β-actin from (Zhongshan Jinqiao, China, 1:1000). The membranes were incubated with the anti-mouse horseradish peroxidase-conjugated secondary antibody (Boster, Wuhan, China, 1:1000). The blots were visualized using an enhanced chemiluminescence kit (Amersham Biosciences, Piscataway, NJ). Densitometry of Western blots was analyzed with Quantity One software and normalized to the respective loading control signal on each blot.

TOF-SIMS analysis for cellular calcification

After the BMSCs were cultured on Blank, PE, PArN, PArNH, and PArNH$_2$ for 7 days, the samples were rinsed with PBS twice, fixed in 4.0 % paraformaldehyde overnight, and washed again with PBS twice. They were dehydrated in a series of ethanol and tert-butanol and freeze-dried for 24 h. TOF-SIMS (TOF-SIMS V from ION-TOF GmbH, Munster, Germany) was conducted and a Bi_1^+ liquid metal ion gun at 30 keV and 45° incident angle was used. The analysis was done on an area of 200 × 200 μm^2 corresponding to 256 × 256 pixels. Charge compensation with an electron flood gun was implemented during

the analysis and the positive ion spectra were calibrated by the C^+, CH^+, C_2^+, and $C_2H_3^+$ peaks.

Statistical analyses

The statistical analysis was conducted using the SPSS version 18.0 (Chicago, IL, USA) software. The data were expressed as means ± SD and $p < 0.05$ was considered statistically significant. The differences between groups were determined by the least significant difference (LSD) test.

Results

Formation and identification of nitrogen functionalities

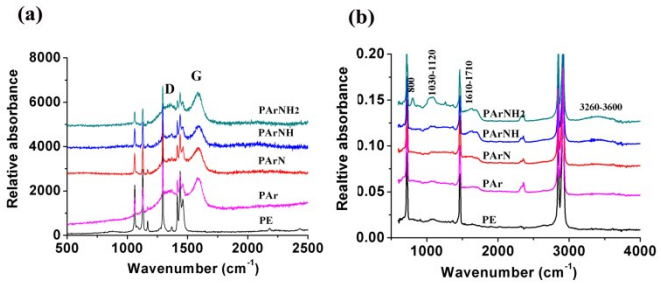

Fig. 1 (a) Raman spectra and (b) ATR-FTIR spectra of PE, PAr, PArN, PArNH, and $PArNH_2$.

The Raman spectra (Fig. 1a) show obvious D and G peaks at 1330 cm^{-1} and 1580 cm^{-1} for PAr, PArN, PArNH, and $PArNH_2$ and similar characteristics as pyrolytic carbon produced by plasma bhysical vapor deposition[26, 27] suggesting that pyrolytic carbon is generated on the PE substrate. Moreover, the grazing incidence angle X ray diffraction analysis shows the generated byrolytic carbon is in little crystal state (Fig. S1†). Generally, the main features of byrolytic carbon are the D, G, and 2D bands at 1330 cm^{-1}, 1580 cm^{-1}, and 2700 cm^{-1}.[28] The broadened D band indicates that there are many structural defects and lack of spatial uniformity and disappearance of the 2D band suggests a lack of spatial uniformity. The G band is often detected from sp^2 systems originating from in plane vibrations and suggests C=C bond formation on PAr, PArN, PArNH, and $PArNH_2$. The lack of stretching vibration peaks between 2280 cm^{-1} and 2210 cm^{-1} indicates the presence of little C≡C bond. Specially, the reduced peaks at 1061 nm, 1130 nm, 1293 nm and 1439 nm assigned to various vibrations of $-CH_2$ do not necessarily imply that the PE molecular structure remains in the pyrolytic carbon of PAr, PArN, PArNH, and $PArNH_2$. It is because the plasma generated structure is thinner than the penetration depth of the evanescent wave used for the measurement since the wavelength of the laser is 532 nm. The absence of signal at 2230 cm^{-1} in Fig. 1b indicates little C≡N bond on the three samples since C≡N absorption is generally strong. Comparing the three samples, little C=N bond is observed after N PIII from PArN at about 1650 cm^{-1}, but larger intensity of C=N bond is found from the PArNH and $PArNH_2$ spectra after additional hydrogen PIII. The larger intensity of the relative multi peaks from 1030 to 1120 cm^{-1} for PArNH to PArN means that more –NH or $-NH_2$ groups are generated by hydrogen PIII. The peak at 800 cm^{-1} and another broad one at 3260-3600 cm^{-1} observed from $PArNH_2$ arises from NH_2 groups become stronger after hydrogen PIII for a long time. The findings demonstrate that hydrogen PIII generates primary amine on $PArNH_2$.

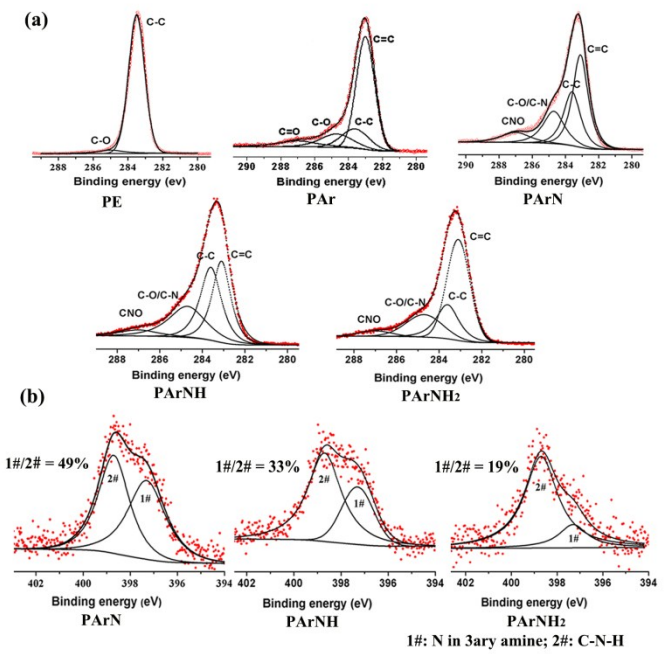

Fig. 2 Deconvoluted XPS spectra of PE, PAr, PArN, PArNH, and $PArNH_2$: (a) C1s and (b) N1s.

Additional information about the surface chemical structure is obtained by XPS using the deconvolution spectra of PAr, PArN, PArNH, and $PArNH_2$ (Fig. 2). The presence of abundant C=C bond (Fig. 2a) indicates that energetic argon ion bombardment breaks the macromolecule chains and sputters H from the C-H bond, but most of C=C bonds remain after subsequent nitrogen and hydrogen PIII. It has been shown that the N1s signal at a binding energy of 398.7 eV is a good indicator of the presence for primary amine.[29-31] Fig. 2b shows two peaks (1# at 397.3 eV, 2# at 398.7 eV) in the N1s spectra associated with N in the tertiary amine and C-N-H bond, respectively. It can be concluded that the amount of tertiary amine decreases from 49% to 19% after hydrogen PIII. In addition, there are many structural defects and lack of spatial uniformity in the byrolytic carbon structure of these three samples and therefore, oxidation occurs to produce C-O, C=O and N-C=O bonds, as shown in Fig. 1b and Fig. 2a. In order to mitigate oxygen incorporation, the samples should be kept in a vacuum.

In order to detect subtle changes in the surface chemistry, TOF-SIMS is again employed to obtain the chemical information (Fig. 3 and Table 1). In the positive spectra acquired from PArN, PArNH, and $PArNH_2$, the decreased intensity of the $C_2H_3^+$ fragment ion at 28 m/z for the PE molecule again indicates that argon PIII sputters the H from $-CH_2$ to generate C=C bond. Compared to PE, the intensity of the C_2H_5, C_3H_7 and C_4H_7 fragments at 29 m/z, 43 m/z, and 55 m/z is weaker on PArN but stronger on PArNH, and $PArNH_2$. It suggests that a great deal of CH_3N, C_2H_5N and C_3H_5N groups at 29 m/z, 43 m/z and 55 m/z are generated by the hydrogen plasma treatment since the nitrogen containing ions are insensitive. The strong peaks at 27 m/z and 41

m/z indicate CHN and C_2H_3N formation on PArN after the nitrogen plasma treatment. The data show that tertiary amine, secondary amine, and primary amine are the major nitrogen functionalities on PArN, PArNH, and $PArNH_2$, respectively, and the amount of primary amine is directly related to the hydrogen PIII time.

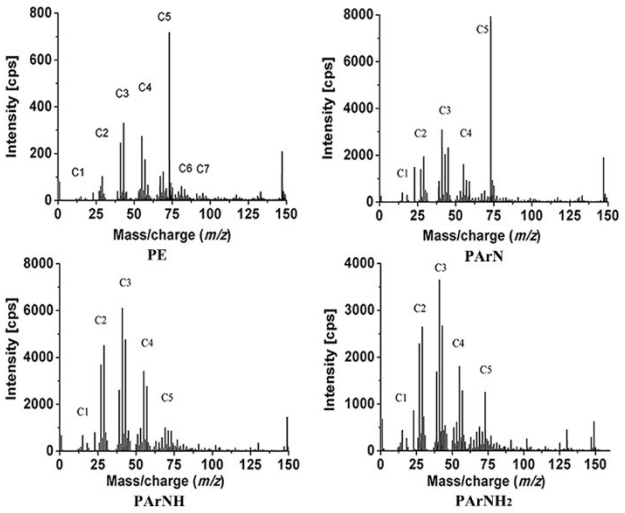

Fig. 3 TOF-SIMS positive spectra of PE, PArN, PArNH, and $PArNH_2$.

Table 1 Relative change of the featured fragment peaks on the TOF-SIMS positive spectra.

	m/z	PE	PArN	PArNH	$PArNH_2$
C1	15	CH_3	CH_3/NH	CH_3/NH↑	CH_3/NH
	27	C_2H_3	C_2H_3/CHN↑	C_2H_3/CHN↑	C_2H_3/CHN↑
	28	C_2H_4	C_2H_4/CH_2N↓	C_2H_4/CH_2N↓	C_2H_4/CH_2N↓
C2	29	C_2H_5	C_2H_5/CH_3N	C_2H_5/ CH_3N↑	C_2H_5/CH_3N↑
	41	C_3H_5	C_3H_5↓	C_3H_5/C_2H_3N↑	C_3H_5/C_2H_3N↑
C3	43	C_3H_7	C_3H_7 /C_2H_5N	C_3H_7/C_2H_5N↑	C_3H_7/C_2H_5N↑
C4	55	C_4H_7	C_4H_7 /C_3H_5N	C_4H_7 /C_3H_5N↑	C_4H_7 /C_3H_5N↑

Notes: "↑" and "↓" indicate the increase and decrease of the featured fragments, respectively.

Surface morphology

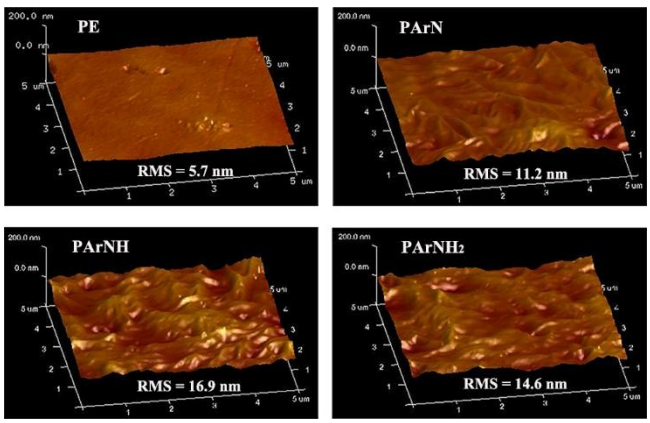

Fig. 4 AFM surface morphological images of PE, PArN, PArNH, and $PArNH_2$.

Fig. 4 reveals that PArN, PArNH and $PArNH_2$ possess similar surface roughness after the PE substrate undergoing a series of PIII processes. Compared to PE, the surface of PArN, PArNH, and $PArNH_2$ shows wrinkles. Two sequential effects are considered to cause the wrinkle surface: (1) ion bombardment resulting in cross linking structure, and (2) during the long cooling time, structural re-organization and contraction of the PE substrate under the pyrolytic carbon films producing interior stress between the substrate and film thereby forming the wrinkles.

Effects of nitrogen functionalities on cell apoptosis and cycle

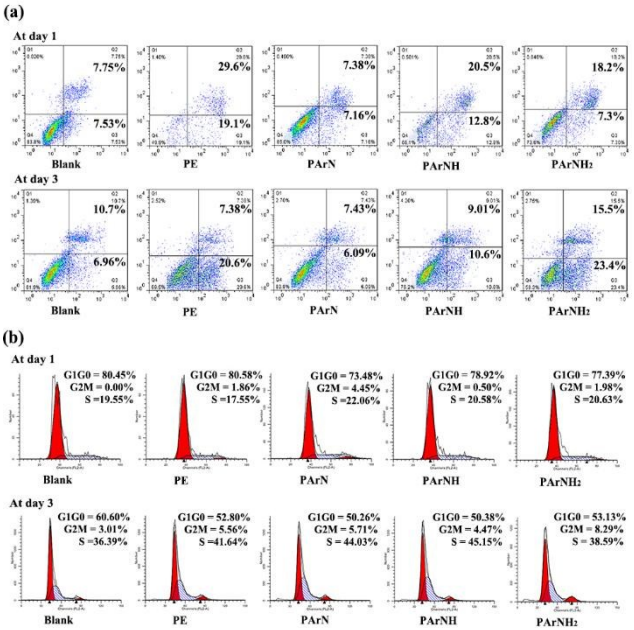

Fig. 5 Analysis of cell apoptosis and cycle of BMSCs cultured on blank, PE, PArN, PArNH and $PArNH_2$ at day 1 and 3: (a) Cell apoptosis and (b) Cell cycle. The figures show the cell state of a representative of three repetitive experiments and 10,000 cells are analyzed.

The FCM results (Fig. 5a) reveal that the viable cells on PArN, PArNH, and $PArNH_2$ are more than those on PE at day 1, implying that all three types of amines can support cell colonization and growth. However, only PArN with tertiary amine exhibits a comparable amount of active cells with the blank, suggesting that tertiary amine has better cytocompatibility to BMSCs than primary and secondary amines in the initial incubation stage. After 3 days, the percentage of apoptotic cells on PArN and blank remains small but more apoptotic cells are detected from $PArNH_2$, further suggesting that tertiary amine can improve cytocompatiblity better than primary and even secondary amine. The results are evidenced by cell proliferation behaviours using MTT assays (Fig. S2†). According to the cell cycle progression of BMSCs (Fig. 5b), comparable numbers of BMSCs on PArN, PArNH and $PArNH_2$ are in the S and G2/M phases as well as blank after incubation for 1 and 3 days. The *in vitro* study indicates that tertiary amine on PArN bodes well for compatibility with BMSC cells although all three types of amines support cell colonization and growth.

Cellular inflammatory effects of nitrogen functionalities

Tumor necrosis factor α (TNF-α) plays a key role in bone regeneration and is also important to inflammatory effects of several cell types.[32,33] To assess the inflammatory effects of primary, secondary, and tertiary

amines on cells, quantitative real time-polymerase chain reaction is performed to detect the mRNA expression levels of TNF-α in BMSCs. Fig. 6 shows that the PE group has the most drastic immunological effects leading to high expression of TNF-α. In contrast, the mRNA expression of TNF-α in PArN, PArNH, and $PArNH_2$ are significantly reduced compared to the blank group. All three types of amines can inhibit the cellular inflammatory effects of cultured BMSCs and exhibit good cytocompatibility with BMSCs. Therefore, low TNF-α expression level shows little inflammatory response to PArN, PArNH, and $PArNH_2$.

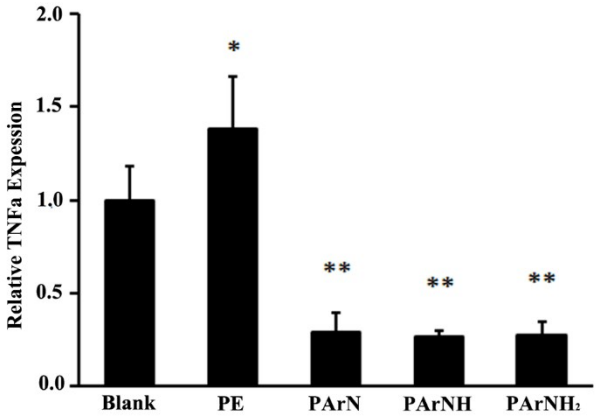

Fig. 6 TNFa expression of BMSCs on blank, PE, PArN, PArNH, and $PArNH_2$ at day 3, relative to GAPDH expression, and normalized to TNFa expression on Blank. Asterisk (*) and (**) denote statistical significance compared to the blank ($p < 0.05$ and $p < 0.01$)

Osteogenesis capability of nitrogen functionalities

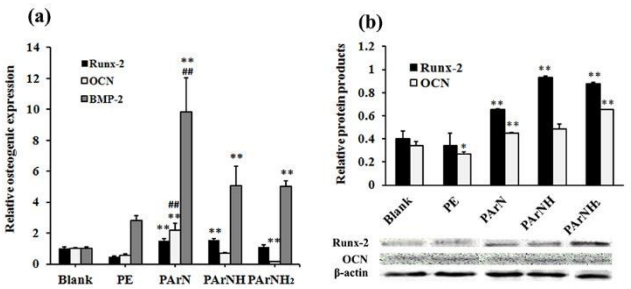

Fig. 7 Effects of nitrogen functionalities on osteogenesis related genes/protein expressions of BMSCs: (a) Expression levels of osteogenic markers at day 3 by quantitative real time-polymerase chain reaction, relative to GAPDH expression and normalized to expressions by cells cultured on the blank. (b) Runx-2 and OCN protein products of cells cultured at day 7 by western blot analysis, relative to β-actin. (**) and (##) denote statistical significance compared with blank and $PArNH_2$, respectively ($p < 0.01$).

The Runt-related transcription factor 2 (Runx-2) is a key transcriptional modulator in the process of mesenchymal stem cell differentiation into osteoblasts.[34] It plays a fundamental role in osteoblast maturation and homeostasis and is essential to normal bone regeneration. Osteocalcin (OCN) and bone morphogenetic brotein 2 (BMP-2), two markers of a mature osteoblast differentiation, are necessary factors for bone calcification and mineralization.[35] Therefore, Runx-2, OCN and BMP-2 related gene/protein expressions can serve as measurement of BMSCs osteogenesis. Fig. 7a shows the expressions of osteogenic markers by quantitative real time-polymerase chain reaction. The increased expressions of Runx-2, OCN, and BMP-2 prove that BMSCs on PArN is induced to differentiate down the osteogenic pathway by tertiary amine. However, PArNH with secondary amine and $PArNH_2$ with primary amine have irregular regulation on cellular osteogenic differentiation. Fig. 7b shows that while there is no change in the protein products on PE, a large increase in the Runx-2 protein relative to the blank is observed from BMSCs on PArN, PArNH and $PArNH_2$. The elevated expressions of Runx-2 and OCN proteins are in accordance with high osteogenic differentiation of cells on PArN. The phenomenon suggests that among the three types of amines, tertiary amine has the greatest capability to upregulate osteogenesis of BMSCs.

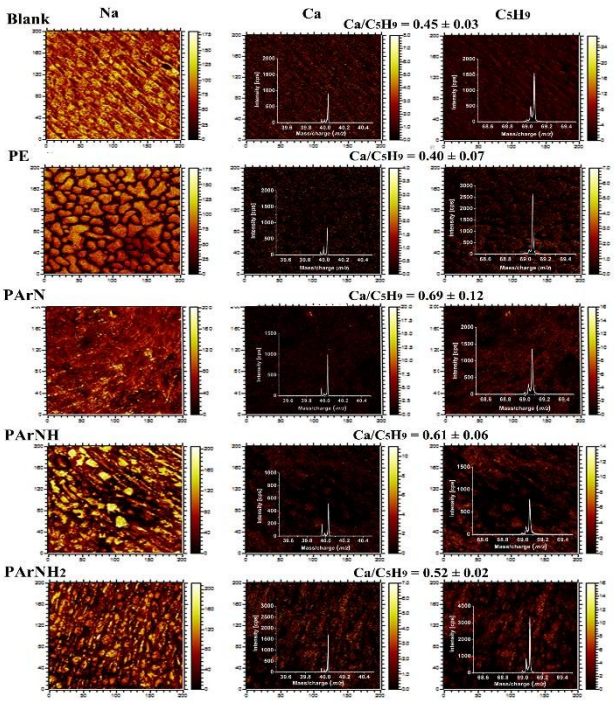

Fig. 8 Effects of nitrogen functionalities on calcification of BMSCs and TOF-SIMS images of BMSCs after culturing on Blank, PE, PArN, PArNH, and $PArNH_2$ for 7 days. The inserted curves are high-resolution spectra of Ca and C_5H_9 ions. The field of view is 200 μm × 200 μm.

Localization of Na ion can be used as a general indicator of the location of the cytosol of a cell.[36-38] The TOF-SIMS images (Fig. 8) disclose that the BMSCs have a spread morphology on PArN, PArNH, and $PArNH_2$, and round morphology on PE, although the cells have already been cultured for 7 days. It unambiguously proves that primary, secondary, and tertiary amines have the capability to increase the biocompatibility of the PE substrate and enhance BMSCs growth, consistent with previous FCM results. Furthermore, the amount of Ca (mass to charge ration m/z = 40) is a specific indicator of cellular calcification due to nitrogen functionalities. The TOF-SIMS images of Ca show that more hydroxyapatite emerges. A mass-to-charge ratio of 69 corresponds to the C_5H_9 fragment ion, an acyl chain fragment from the membrane phospholipids in individual cell. The density and distribution of the C_5H_9 fragment ion show the number and total phospholipid distribution of BMSCs on the surfaces.[38] The Ca level normalized to C_5H_9 ion indicates the calcification ability of cells

without interference by the cell number. The high-resolution spectra of Ca and C_5H_9 ions are also depicted in Fig. 8. They clearly reveal that the BMSCs have larger mineral concentrations on PArN, PArNH, and $PArNH_2$ than blank and PE. In particular, the Ca ions decrease from PArN to PArNH and $PArNH_2$, meaning that tertiary amine possessse the optimal capability to direct osteogenesis of BMSCs. All in all, the gene expression, protein production, and cell calcification levels demonstrate that primary, secondary and tertiary amines have positive influence on signaling BMSCs to differentiate down the osteogenic pathway and of the three, tertiary amine has the greatest capability to promote osteogenesis of BMSCs.

Discussion

Nitrogen containing groups prepared by plasma technology show good cytocompatibility[19, 39] and can even enhance osteogenic differentiation of bone cells.[19] For instance, T. Yokota found that cell adhesion on nitrogen-doped DLCs increased monotonically with nitrogen concentration in the film.[14] They believed that the better cellular adhesion and proliferation on the modified surface were mainly attributed to enhancement of the extracellular matrix (ECM) protein adhesion to these nitrogen containing groups.[40] However, it was not clear which nitrogen functionality played the critical role in promoting cytocompatibility and signaling osteogenesis. Abhijit Majumdar reported that a nitrogen plasma-deposited coating showed heavy cytotoxicity to cells in contact and larger amounts of nitrogen in the film accelerated cell death.[22] The effects of nitrogen functionalities on bone cells are therefore ambiguous and sometimes contradictory. The complex plasma reaction and polymer chemistry make it difficult to controllably generate the selected nitrogen functionalities to attain the desirable biological outcome. Therefore, it is necessary to design a plasma modification protocol to controllably construct different types of nitrogen functionalities in order to evaluate the individual biological effects. Our study demonstrates that argon plasma bombardment dissociates the inherent chemical bonds and generates pyrolytic carbon as the platform to controllably generate nitrogen functionalities including primary, secondary, and tertiary amines using subsequent nitrogen or hydrogen PIII. Raman scattering, ATR-FITR, XPS, and TOF-SIMS reveal that on the single and uniform carbonaceous structure, only nitrogen PIII generates the tertiary amine group. After additional hydrogen PIII, the major nitrogen functionalities gradually vary from tertiary amine to secondary and primary amines (Figs. 2 and 3). Consistent with our objective, the three types of amines can be fabricated controllably by nitrogen and hydrogen PIII making it possible to identify the biological effects of individual nitrogen functionalities and identify the optimal chemical structure from the perspective of cytocompatibility and osteogenesis of BMSCs.

The BMSCs are capable of both self renewal and differentiation into multiple cell lineages.[34] The local microenvironment such as surface chemical groups,[5] area, and topography[41] can significantly affect the biological functions of BMSCs. AFM reveals that PArN, PArNH, and $PArNH_2$ have similar surface morphology implying that surface chemistry is the major factor affecting the cells. Therefore, FCM is carried out to study effects of three types of amines on the viability, apoptosis, and proliferation of BMSCs. The results demonstrate that tertiary amine has the better capability of retaining the cell viability while inhibiting apoptosis of BMSCs than primary and secondary amines. Studies of the TNF-α release related to the immunogenic response is determined to assess the potential in various biomedical and tissue engineering applications. All three types of amines are found to be low in inflammatory response and TNF-α value and comparable to cell culture plates. Hence, all three types of amines generated by plasma technology can endow the substrate with good cytocompatibility and tertiary amine shows the highest efficiency in avoiding inflammation and initiating the reparative phase concurrently.

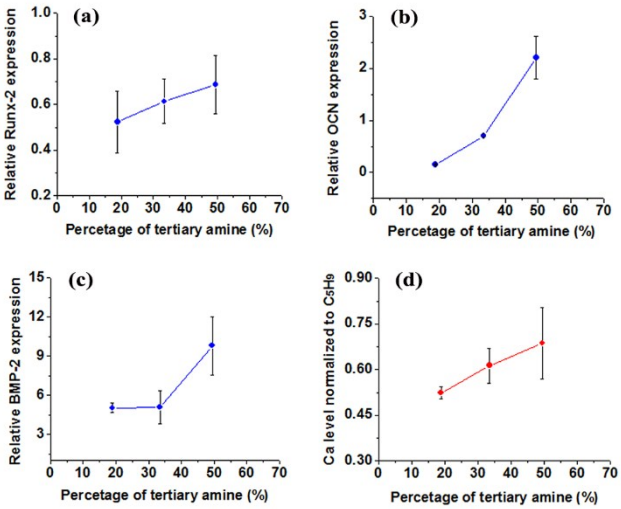

Fig. 9 Effects of tertiary amine on BMSCs osteogenesis: (a) runx-2 gene, (b) OCN gene, (c) BMP-2 gene, and (d) Ca level normalized to C_5H_9.

Generally, BMSCs can undergo osteoinduction *in vitro*, and their differentiation and maturation into osteoblasts have three major stages: cell proliferation, matrix maturation, and mineralization.[34] The differentiation process includes directional differentiation of multipotent stromal cells into preosteoblasts, immature osteoblasts, and mature osteoblasts. The osteoblast cells predominantly express extracellular matrix proteins such as Runx-2, OCN and BMP-2 during the cell proliferation, matrix maturation, and mineralization phases. Observation of the mRNA expression levels of these marker genes helps to distinguish the stages of differentiation and maturation of BMSCs affected by primary, secondary and tertiary amines into osteoblasts. Previous studies[6, 35] have shown that Runx-2 is secreted during the early stage of osteogenic differentiation, whereas OCN and BMP-2, two markers of a mature osteoblast differentiation, are necessary factors of bone calcification and mineralization. It is a mineralized tissue specific protein that is expressed in differentiated osteoblasts and appears to function in the initial mineralization of bone. In this study, expression of bone related genes, including Runx 2, OCN and BMP-2, are upregulated in only the PArNH-BMSCs culture, but in PArNH-BMSCs and $PArNH_2$-BMSCs all the genes expression do not change significantly compared to the blank. Moreover, the expression level of three bone related genes is positively correlated with the percentage of tertiary amine in the nitrogen plasma modified surface, as shown in Figs. 9a, b and c. Therefore, it is believed that tertiary amine plays a critical role in

upregulation osteogenesis of BMSCs. By checking the Runx 2 and OCN protein levels, the BMSCs are collected from PArN, PArNH and $PArNH_2$ at day 7 which represents the matrix maturation stage of osteogenic differentiation. In this stage, the ECM and stem cell function are kept in balance. The Runx 2 and OCN protein levels in PArNH and $PArNH_2$, except PArN, are also upregulated and it is different from the mRNA expression. One possible explanation is that the signaling pathways can affect the Runx 2 function by activating enzymes that post translationally modify Runx 2 and/or by mobilizing cofactors that interact with Runx 2 to either positively or negatively regulate the DNA binding or transcriptional activities. The irregular expression level of Runx 2/OCN genes/proteins on PArNH and $PArNH_2$ demonstrates that primary and secondary amines have small capability in modulating BMSCs osteogenesis.

rotein 2 studies involving the use ALP or Alizarin red staining to detect the osteogenic differentiation ability of stem cells, 14 to 21 days were needed and the results were not too accurate. TOF SIMS is surface sensitive mass spectrometric technique to monitor calcification of BMSCs cultured on the samples in the early stage.[36, 38] As shown by the high resolution spectra of Ca and C_5H_9, BMSCs have larger mineral concentrations on PArN, PArNH, and $PArNH_2$ than the blank and PE. Fig. 9d shows that calcification level decreases with decreasing percentage of tertiary amines on the surface (PArN > PArNH > $PArNH_2$) demonstrating that tertiary amine possesses the greatest capability to upregulate BMSCs osteogenesis. As it known, amine groups (especially, tertiary amines) are prone to be protonated at biological pH of 7.5, thus their surface exhibits positively charged in cell culture media. Consequently, the plasma modified surface with tertiary amines possibly offers a local biochemical and electrostatic environment to BMSCs, and stimulates and guides them to differentiate down to osteogenesis. This hypothesis is partially evidenced by the facts that the positively charged materials have been shown to specifically direct BMSCs to differentiate to accomplish osteogenesis and promote bone regeneration.[42-45] The hidden mechanism will be our focus in the future research. In summary, the ability to selectively produce a large percentage of tertiary amine on a polymeric implant by the plasma technology described in this paper facilitates not only osseointegration, but also mitigate foreign body reactions.

Conclusions

A strategy to controllably construct nitrogen functionalities on polymers by plasma immersion ion implantation is described. Argon PIII is first conducted to convert the polymer surface into pyrolytic carbon and ensuing nitrogen and hydrogen PIII selectively produces primary, secondary and tertiary amine groups. The samples provide the platform to probe the unique effects of nitrogen functionalities on BMSC cells. Our results show that on the pyrolytic carbon, other nitrogen functionalities such as NH_2 can be generated by increasing the hydrogen amount in the implanted ions. Because of the excellent control on the nitrogen functionalities, it probes that the tertiary amine has the optimal efficiency pertaining to mitigating foreign body reactions and signaling osteogenesis related gene/protein and calcification of BMSCs. Plasma technology is thus excellent in providing the proper chemical microenvironment for BMSCs to promote osteogenesis on orthopedic polymers.

Acknowledgments

Financial support from the National Natural Science Foundation of China (NSFC 51473175, 51103170), Chinese Academy of Sciences, City University of Hong Kong Strategic Research Grant (SRG) No. 7004188, City University of Hong Kong Applied Research Grant (ARG) No. 9667085, and Hong Kong Research Grants Council (RGC) General Research Funds (GRF) No. CityU 112212 is acknowledged.

Notes and references

[a] Technical Institute of Physics and Chemistry, Chinese Academy of Sciences, Beijing 100190, China. Fax: +86-10-82543776, Tel: +86-10-82543776, Email: weizhang@mail.ipc.ac.cn and jhji@mail.ipc.ac.cn
[b] Stomatology Department of the General Hospital of Chinese PLA, 28 FuXing Road, Beijing 100853, China
[c] Department of Physics & Materials Science, City University of Hong Kong, Tat Chee Avenue, Kowloon, Hong Kong, China
† Electronic supplementary information (ESI) available: Experimental data, Fig. S1–S2. See DOI: 10.1039/c000000x/

1. D. Puppi, F. Chiellini, A. M. Piras and E. Chiellini, *Prog. Polym. Sci.*, 2010, **35**, 403-440.
2. M. Prewitz, F. P. Seib, T. Pompe and C. Werner, *Macromol. Rapid Comm.*, 2012, **33**, 1420-1431.
3. R. P. Robinson and T. M. Green, *J. Arthroplasty.*, 2011, 26, 1165-1169.
4. Y. Kosashvili, D. Backstein, O. Safir, D. Lakstein and A. E. Gross, *J. Arthroplasty.*, 2011, **26**, 1170-1175.
5. D. S. W. Benoit, M. P. Schwartz, A. R. Durney and K. S. Anseth, *Nat. Mater.*, 2008, **7**, 816-823.
6. M. P. Lutolf, P. M. Gilbert and H. M. Blau, *Nature*, 2009, **462**, 433-441.
7. S. B. Goodman, Z. Yao, M. Keeney and F. Yang, *Biomaterials*, 2013, **34**, 3174-3183.
8. E. Kaivosoja, G. Barreto, K. Levon, S. Virtanen, M. Ainola and Y. T. Konttinen, *Ann. Med.*, 2012, **44**, 635-650.
9. A. Y. Chen, Z. Deng, A. N. Billings, U. O. Seker, M. Y. Lu, R. J. Citorik, B. Zakeri and T. K. Lu, *Nat. Mater.*, 2014, **13**, 515-523.
10. F. R. Maia, S. J. Bidarra, P. L. Granja and C. C. Barrias, *Acta Biomater.*, 2013, **9**, 8773-8789.
11. S. Mitragotri and J. Lahann, *Nat. Mater.*, 2009, 8, 15-23.
12. D. V. Bax, Y. Wang, Z. Li, P. K. Maitz, D. R. McKenzie, M. M. Bilek and A. S. Weiss, *Biomaterials*, 2011, **32**, 5100-5111.
13. T. Pompe, K. Keller, G. Mothes, M. Nitschke, M. Teese, R. Zimmermann and C. Werner, *Biomaterials*, 2007, **28**, 28-37.
14. T. Yokota, T. Terai, T. Kobayashi, T. Meguro and M. Iwaki, *Surf. Coat. Tech.*, 2007, **201**, 8048-8051.
15. W. Zhang, Y. Luo, H. Wang, J. Jiang, S. Pu and P. K. Chu, *Acta Biomater.*, 2008, **4**, 2028-2036.
16. R. A. N. Pertile, F. K. Andrade, C. Alves and M. Gama, *Carbohyd. Polym.*, 2010, **82**, 692-698.
17. L. Garrido, I. Jiménez, G. Ellis, P. Cano, J. M. García-Martínez, L. López and E. de la Peña, *J. Appl. Polym. Sci.*, 2011, **119**, 3286-3296.

18. H. Wang, M. Xu, Z. Wu, W. Zhang, J. Ji and P. K. Chu, *ACS Appl. Mater. Inter.*, 2012, **4**, 4380-4386.
19. Z. Gugala and S. Gogolewski, *J. Biomed. Mater. Res. A*, 2006, **76**, 288-299.
20. L. C. Lopez, M. R. Belviso, R. Gristina, M. Nardulli, R. d'Agostino and P. Favia, *Plasma Process. Polym.*, 2007, **4**, S402-S405.
21. F. J. Harding, L. R. Clements, R. D. Short, H. Thissen and N. H. Voelcker, *Acta Biomater.*, 2012, **8**, 1739-1748.
22. A. Majumdar, K. Schröder and R. Hippler, *J. Appl. Phys.*, 2008, **104**, 074702.
23. F. Liu, B. Li, J. Sun, H. Li, B. Wang and S. Zhang, *Appl. Surf. Sci.*, 2012, **258**, 4322-4327.
24. F. Mwale, H. T. Wang, V. Nelea, L. Luo, J. Antoniou and M. R. Wertheimer, *Biomaterials*, 2006, **27**, 2258-2264.
25. C.-S. Wang, G.-H. Tong, H.-C. Chen, W.-C. Shih and I. N. Lin, *Diam. Relat. Mater.*, 2010, **19**, 147-152.
26. L. Xu, J. Wu and S. Bai, *Carbon*, 2012, **50**, 4705-4710.
27. W. J. Lee, C. e. Li, J. Gunning, N. Burke and J. Patel, *Carbon*, 2012, **50**, 4773-4780.
28. N. McEvoy, N. Peltekis, S. Kumar, E. Rezvani, H. Nolan, G. P. Keeley, W. J. Blau and G. S. Duesberg, *Carbon*, 2012, **50**, 1216-1226.
29. W. Ding, Y. Okabe, W. Chai and D. Ju, *Surf. Coat. Tech.*, 2011, **205**, 5318-5323.
30. J. Hanuš, G. Ceccone and F. Rossi, *Plasma Process. Polym.*, 2012, **9**, 371-379.
31. K. Kereszturi, A. Tóth, M. Mohai, I. Bertóti and J. Szépvölgyi, *Appl. Surf. Sci.*, 2010, **256**, 6385-6389.
32. W. Niedbala, J. C. Alves-Filho, S. Y. Fukada, S. M. Vieira, A. Mitani, F. Sonego, A. Mirchandani, D. C. Nascimento, F. Q. Cunha and F. Y. Liew, *P.Natl. Acad. Sci.*, 2011, **108**, 9220-9225.
33. Y. Moriyama, E. H. Moriyama, K. Blackmore, M. K. Akens and L. Lilge, *Photochem. Photobiol.*, 2005, **81**, 1351-1355.
34. C.-L. Tsai, P.-C. Wu, M. E. Fini and S. Shi, *Invest. Ophth. Vis. Sci.*, 2011, **52**, 5481-5487.
35. M. Alcaide, M. C. Serrano, R. Pagani, S. Sanchez-Salcedo, M. Vallet-Regi and M. T. Portoles, *Biomaterials*, 2009, **30**, 45-51.
36. J. Brison, M. A. Robinson, D. S. Benoit, S. Muramoto, P. S. Stayton and D. G. Castner, *Anal. Chem.*, 2013, **85**, 10869-10877.
37. C. Szakal, K. Narayan, J. Fu, J. Lefman and S. Subramaniam, *Anal. Chem.*, 2011, **83**, 1207-1213.
38. S. G. Ostrowski, C. T. Van Bell, N. Winograd and A. G. Ewing, *Science*, 2004, **305**, 71-73.
39. F. Mwale, H. T. Wang, V. Nelea, L. Luo, J. Antoniou and M. R. Wertheimer, *Biomaterials*, 2006, **27**, 2258-2264.
40. C. C. Barrias, M. C. L. Martins, G. Almeida-Porada, M. A. Barbosa and P. L. Granja, *Biomaterials*, 2009, **30**, 307-316.
41. P. Rompolas, K. R. Mesa and V. Greco, Nature, 2013, **502**, 513-519.
42. Y.L. Qu, Y.Y. Wang, X.L. Kong, J.D. Li, Y. Zuo, P. Gong and Y. Man. *J. Biomater. Sci-Polym. Ed.*, 2014, **25**, 211-223.
43. Wang Y, et al. Y.Y. Wang, R. Shi, P. Gong, J.D. Li, J. Li, D.T. Ao, P. Wang, Y. Yang, Y. Man and Y.L. Qu. *J. Bioact. Compat. Pol.*, 2012, **27**, 122-132.
44. R.R. Costa and J.F. Mano. *Chem. Soc. Rev.*, 2014, **43**, 3453-3479.
45. T.Q. Liao, M.D. Moussallem, J. Kim, J.B. Schlenoff and T. Ma. *Biotechnol. Prog.*, 2010, **26**, 1705-1713.

Effects of Plasma-Generated Nitrogen Functionalities on Upregulation of Osteogenesis of Bone Marrow-Derived Mesenchymal Stem Cells

Wei Zhang,* Jun Liu, Haigang Shi, Na Liu, Kun Yang, Lianxin Shi, Bin Gu, Huaiyu Wang, Junhui Ji,* Paul K. Chu

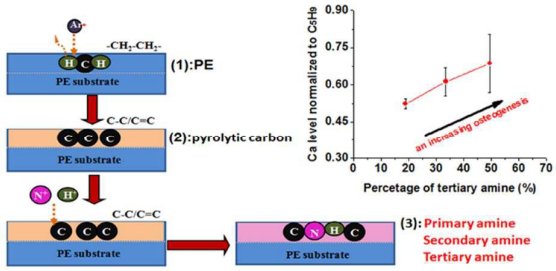

Tertiary amine constructed controllably by plasma technology possesses the optimal capability to promote BMSCs osteogenesis.